SAND2015-2006J

Degradation of different elastomeric polymers in simulated geothermal environments at 300°C

Toshifumi Sugama
Tatiana Pyatina
Sustainable Energy Technologies Department
Brookhaven National Laboratory
Upton, NY 11973-5000

Erica Redline
James McElhanon
Douglas Blankenship
Sandia National Laboratories
PO Box 5800
Albuquerque NM 87185

Abstract

This study evaluates the degradation of six different elastomeric polymers used for O-rings: EPDM, type I- and II-FKM, FEPM, FFKM, and FSR, in five different simulated geothermal environments at 300°C: 1) non-aerated steam/cooling cycles, 2) aerated steam/cooling cycles, 3) water-based drilling fluid, 4) CO_2-rich geo-brine fluid, and, 5) heat-cool water quenching cycles. The factors assessed included the extent of oxidation, changes in thermal behavior, micro-defects, permeation of ionic species from the test environments into the O-rings, silicate-related scale-deposition, and changes in the O-rings' inverse tensile compliance.

The reliability of the O-ring to maintain its integrity depended on the elastomeric polymer composition and the exposure environment. FSR disintegrated while EPDM was oxidized only to some degree in all the environments, FKM withstood heat-water quenching, FEPM survived in all the environments with the exception of heat-water quenching where it underwent severe oxidation-induced degradation, and FFKM displayed outstanding compatibility with all the tested environments. The paper discusses the mechanisms of the elastomers' degradations.

1. Introduction

Elastomeric materials used as non-metallic pump bearings in geothermal environments offer several advantages in comparison with the metallic bearings. Firstly, they can be lubricated with water instead of oil, abating environmental issues. Secondly, they possess high resilience and stiffness, absorbing impact- or shock-loads without permanent deformation. Thirdly, these materials have low friction and excellent corrosion-resistance. Finally, their original dimensions are readily restored after localized deflections caused by passing mineral particles.

Fluoroelastomers are of particular interest because of their thermal resistance, demonstrated both in laboratory and field studies [1-3]. However, for geothermal applications such as submerged pumps, a combination of thermal and chemical stability of elastomers is necessary. Several studies have focused on chemical degradation of FKM in aggressive aqueous environments [1, 4-6]. They revealed de-crosslinking, formation of carbonyl group followed by backbone cleavage, [6] and reactions with metal cations such as Na^{+}, $Fe^{2+,}$ Mg^{2+}, and Ca^{2+}, present in geo-fluid, with the formation of polyfluorocarboxylate complexes with scale deposition on the surface [4]. Such sensitivity to the chemical environment compromised the thermal stability and mechanical properties of the elastomer.

On the other hand, there are many different-types of commercial fluorocarbon-based elastomeric materials that can withstand temperatures above 200°C [7-10]; among them are type II FKM terpolymers, consisting of polyvinylidene fluoride (VDF), hexafluoropropylene (HFP), and tetrafluoroethylene (TFE), the type III FKM tetrapolymer, comprising VDF, HFP, TFE, and perfluoromethylvinylether (PMVE), the FEPM copolymer consisting of TFE and propylene (P), the fluorosilicone copolymer (FSR) composed of polysiloxane (PS) and

trifluoropropylpolysiloxane (TFPPS), and the perfluorocarbon copolymer (FFKM) that includes TFE and PMVE. Further, some geothermal wells have down-hole temperatures over 250°C in addition to harsh chemical environments containing highly concentrated corrosive $CO_{2\,(g)}$- and $H_2S_{(g)}$-derived acids. Drilling tool components, such as O-rings, gaskets, seals, and packers, are exposed not only to environments containing these corrosive gasses, but also encounter water-based drilling fluids, which contain organic compounds, in the down-hole well reservoir [11].

To the best of authors' knowledge there are no general publications with systematic analyses of degradation and stability of different fluorocarbon-based elastomers under the geothermal environments. The present study focused on investigating and evaluating the stability and degradation of O-rings made with fluorocarbon-based elastomeric polymers, such as types I and II FKMs, FEPM, FFKM, and FSR polymers, after direct exposure (without compression) to five different simulated geothermal environments at 300°C: 1) drilling fluid, 2) CO_2-rich reservoir brine fluid, 3) aerated steam/cooling cycles, 4) non-aerated (under N_2 environment) steam/cooling cycles, and, 5) heating in air/water quenching thermal shock. For comparison, the ethylene propylene diene monomer (EPDM) polymer, consisting of a poly(ethylene-*co*-propylene-*co*-5-ethylidene-2-norbornene) terpolymer structure, also was studied as an example of a non-fluorocarbon elastomeric O-ring. The investigated factors included: the extent of oxidation, identification of oxidation derivatives, chemical structure-transformation, thermal stability, morphological alteration, micro-defects, permeation-depth profile of the ionic species through the O-ring, and changes in mechanical properties. Obtaining information on these factors was accomplished using ATR-FTIR, TGA, micro-energy dispersive X-ray, and modulus profile testing, in conjunction with visual observations of the changes in the O-ring's appearance.

2. Experimental procedures

2.1. Materials

Five different elastomeric polymer-based O-rings were supplied by Precision Associates, Inc. Among these were ploy(ethylene-*co*-propylene-*co*-5-ethylidene-2-norbornene, EPDM) terpolymer, poly[vinylidene fluoride (VDF)-*co*- hexafluoropropylene (HFP), type I FKM] copolymer, poly[vinylidene fluoride (VDF)-*co*- hexafluoropropylene (HFP)-*co*-tetrafluoroethylene (TFE), type II FKM] terpolymer, poly[tetrafluoroethylene (TFE)-*co*-propylene (P), FEKM] copolymer, and poly[tetrafluoroethylene (TFE)-*co*-perfluoromethylvinylether (PMVE), FFKM] copolymer. Stockwell Elastomirics, Inc. supplied the O-ring made with fluorosilicone (FSR) consisting of poly[siloxane (PS)-*co*-trifluoropropylpolysiloxane (TFPPS)] copolymer. Figure 1 shows the chemical structures.

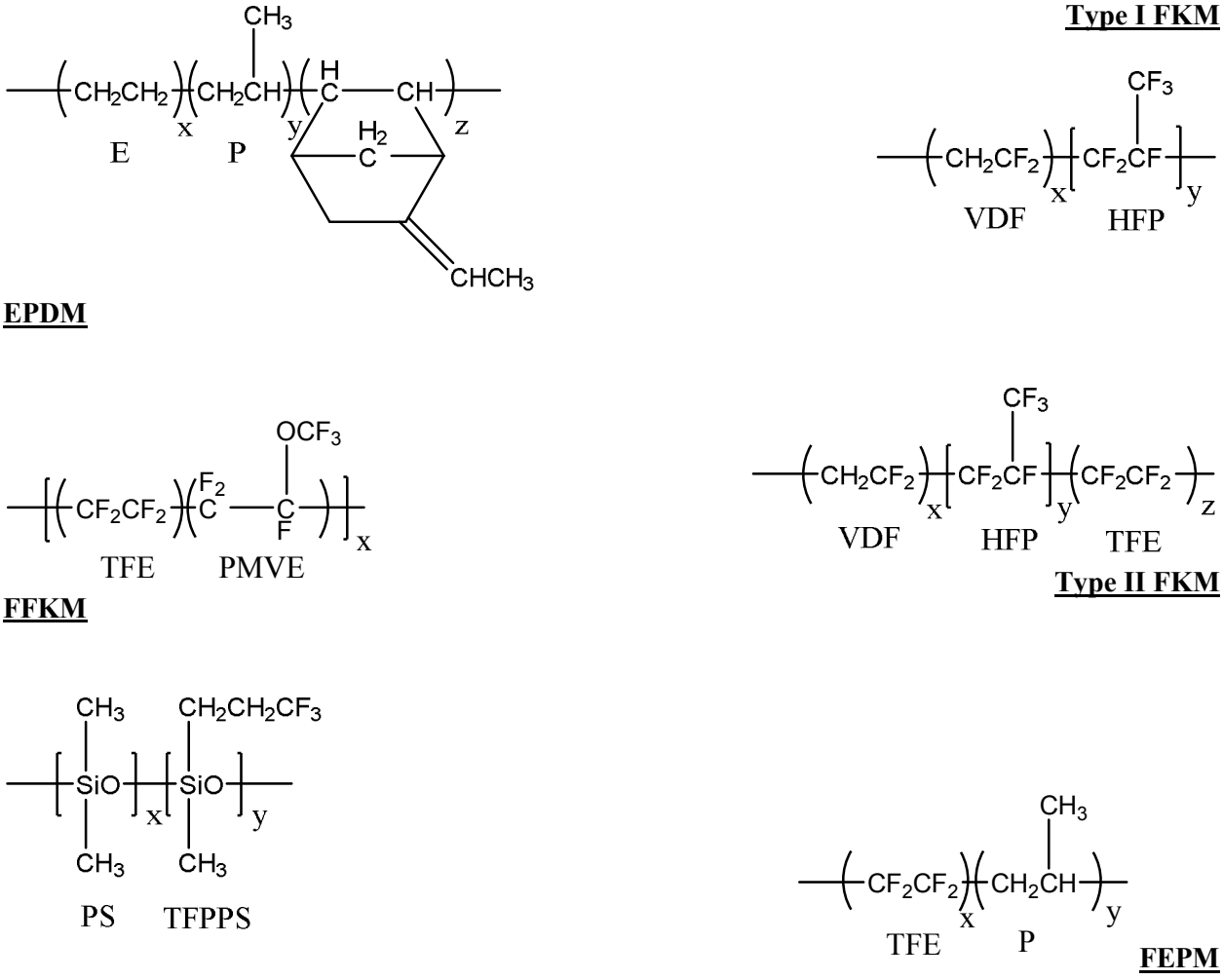

Figure 1. Chemical structures of the various elastomeric polymers used in the study.

2.2. Measurements

Five different exposure environments were employed in this work (Table 1): The first, denoted as No. 1, was 5-cycle 300°C-24 hr non-aerated ($N_{2\ (g)}$ saturated) steam/-25°C cooling; the No. 2 was 5-cycle 300°C-24 hr aerated steam/25°C cooling; the third, No. 3, was exposure in water-based drilling fluid (pH 9-10) at 300°C for 7 days; fourth, No. 4, was immersion in CO_2-rich geo-brine fluid (pH 4-5) at 300°C for 7 days (composition of the brine along with the compounds used to prepare it are given in Table 2; all the chemicals were provided by Sigma-Aldrich); and, fifth (No. 5) was 5-cycle thermal shock (one cycle: 300°C air heating for 24 hrs in an oven and then placing the 300°C-heated samples directly into 25°C water. (Note that deionized water was used for all the tests.)) Details of the first testing procedure were as follows. The O-rings were hung in the head space of an autoclave filled with D.I. water at 30% of the total volume and sealed. The air in the headspace was replaced with N_2, and the temperature was brought up to

300°C. After 24 hours the autoclave was cooled to room temperature at the rate of 50°C/hour. This steam/cooling process was repeated 5 times. The same procedure was used for No. 2 environment, except that the air remained in the head space of the autoclave so the steam was aerated. All the O-rings after the No. 3 and 4 exposures were physically cleaned with a D.I. water-soaked napkin to remove any non-adhering contaminants from their surfaces. All O-rings were dried in an oven at 90°C for 24 hours before conducting the post-test analyses. The compositions of the simulated drilling and geo-brine fluids employed in this study can be found in Tables 1 and 2, respectively.

Table 1. Composition of the simulated drilling fluid

Major Component	**Percent**
Water	74 – 83
Barite	10 – 15
Bentonite	5 – 7
Caustic soda	0.3
Soda ash	1
Polyanionic cellulose	0.3 – 1.2
Xanthan gum	0.3 – 0.5
Starch	0.5 – 1

Table 2. Composition of the simulated geo-brine fluid

Major Components	**Compounds**	**Percent**
Cl^-	NaCl	13.5
Na^+		6
Ca^{2+}	$CaCl_2$	2
K^+	KCl	1.5
Mg^{2+}	$MgCl_2$	0.9
Minor Components		**PPM**
CO_2	$NaHCO_3$	15,000
Fe^{2+}	$FeCl_2$	1000
Mn^{2+}	$MnCl_2$	930
Li^+	LiCl	410
Zn^{2+}	$ZnCl_2$	370
B^{3+}	H_3BO_3	330
Si^{4+}	Na_2SiO_3	250
Ba^{2+}	$BaCl_2$	130
H_2S	H_2SO_4	70

Attenuated Total Reflectance-Fourier Transform Infrared Spectroscopy (ATR-FTIR) was used to identify the oxidation derivatives that were incorporated into polymeric elastomers exposed to these environments and to assess the alterations in their chemical structures. To obtain

information on thermal-, hydrothermal-, and chemical-stabilities and the extent of oxidation, Thermo Gravimetric Analysis (TGA) at the heating rate of 20°C/min in a N_2 flow was employed. A micro energy-dispersive X-ray spectrometer (μEDX) was used to explore whether these environments created micro-defects in O-rings, and to investigate the permeation depth of the ionic species from drilling and geo-brine fluids through O-rings.

To characterize changes in the stiffness of the O-rings exposed to different environments, elastic modulus profiles of each aged specimen were taken using a home-built instrument. The machine operates by scanning the surface with a parabolic tip at user-defined intervals (in this case, 0.2 mm) and uses displacement from a known force applied to each point on a sample to calculate inverse tensile compliance, which is proportional to the tensile (elastic) modulus [12]. Sample preparation included cross-sectioning O-rings, embedding the materials in epoxy, and polishing with a polishing wheel to achieve a smooth surface.

3. Results and discussion

3.1. ATR-FTIR analysis

3.1.1. EPDM

Figure 2 shows the ATR-FTIR absorption spectra in region of 4000 to 650 cm^{-1}, and the appearance of O-rings for EPDM exposed to No. 1 through No. 5 environments. The spectrum for the control encompasses four absorption bands: those at 2919 and 2846 cm^{-1} are due to the C-H asymmetric ($V_{as\,C\text{-}H}$), and symmetric ($V_{s\ C\text{-}H}$) stretching vibrations, respectively, and those at 1453 and 1367 cm^{-1} are from $–CH_2$- scissoring (δ_{CH2}) and $-CH_3$ asymmetric bending (δ_{asCH3}) vibrations [13,14]. There were no visible changes in the appearance of the EPDM O-ring after the non-aerated ($N_{2\ gas}$) steam/cooling testing. New bands assigned to carboxylate, COO^-, asymmetric (V_{asCOO^-}) stretching vibration [15-17] appeared in the region of 1580-1530 cm^{-1}. The result was similar for the treatment in the No. 2 environment (Figure 1(c)). Thus, EPDM O-rings appeared to undergo some oxidation during both the non-aerated- and aerated-steam/cooling cycle tests.

As is evident in the photos, the O-rings exposed to drilling fluid and geo-brine (Figure 1 (d) and (e)) displayed excellent integrity; in contrast, they disintegrated during the thermal-shock tests (f). In particular, it was very difficult to recognize the presence of C-H-related bands at 2919 and 2846 cm^{-1}, demonstrating the rupture of EPDM backbone hydrocarbon chains. The spectrum with very low peak absorbance suggests that the polymer released volatile derivatives that escaped the sample, leaving behind non-volatile residuals, mostly carbon. In contrast, the C-H bands at 2919 and 2846 cm^{-1} still were observed in the samples exposed in No. 3 drilling fluid and No. 4 geo-brine fluid, despite the presence of oxidation-induced COO^- band at 1536 cm^{-1} and the appearance of C=C stretching ($V_{C=C}$) vibration at 1634 cm^{-1} [18]. Additionally, the

prominent band at 1014 cm^{-1} perhaps was due to the precipitation of a silicate (bentonite or other)-related scale layer [19,20] on the surfaces of the O-rings during the exposure. These scales seemed to adhere well to the O-ring surfaces. Thus EPDM was susceptible to oxidation reactions, particularly during the thermal-shock testing.

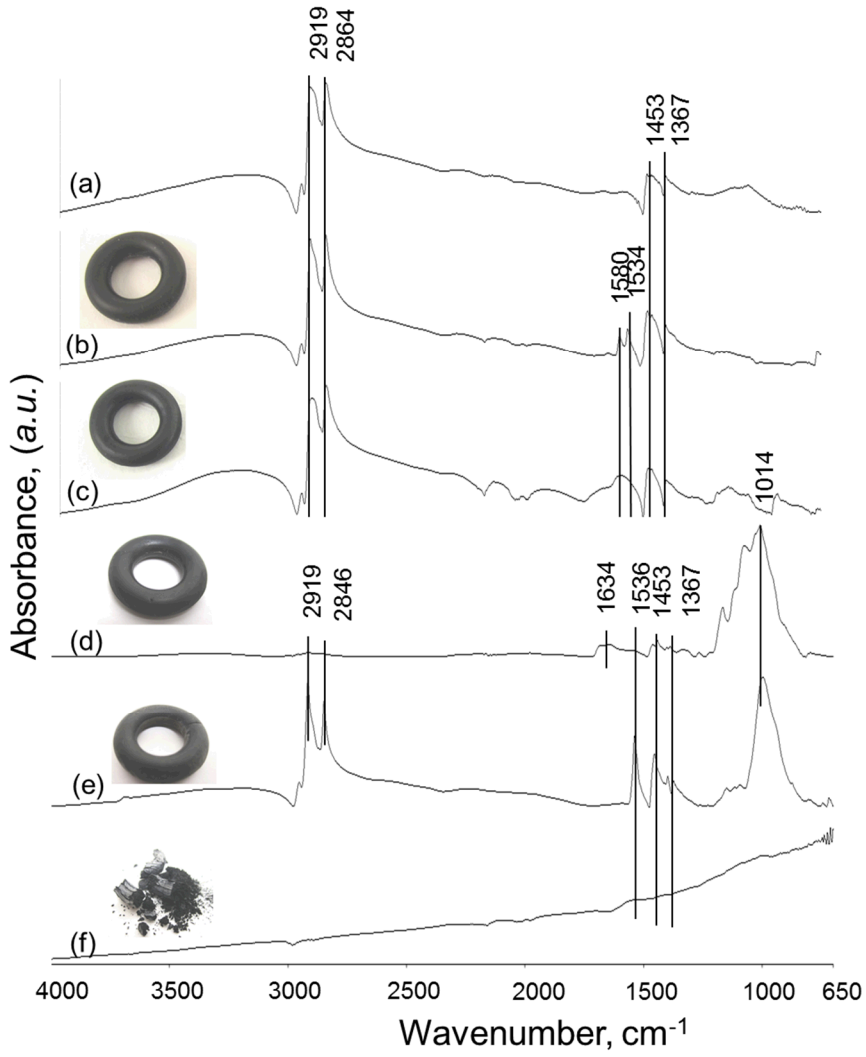

Figure 2. ATR-FTIR absorption spectra and appearance of EPDM O-rings before (a) control, and after**:** (b) No. 1 non-aerated (N_2), (c) No. 2 aerated steam/cooling cycles, (d) No. 3 drilling fluid, (e) No. 4 geo-brine fluid, (f) No. 5 thermal shock tests.

These results are in agreement with reference [18], which suggests degradation involving oxygen incorporation and chain scissions, followed by reactions with the free radicals and deposition of derivatives of each polymeric section of the poly(ethylene-*co*-propylene-*co*-5-ethylidene-2-norbornene) EPDM terpolymer structure (Figure 3).

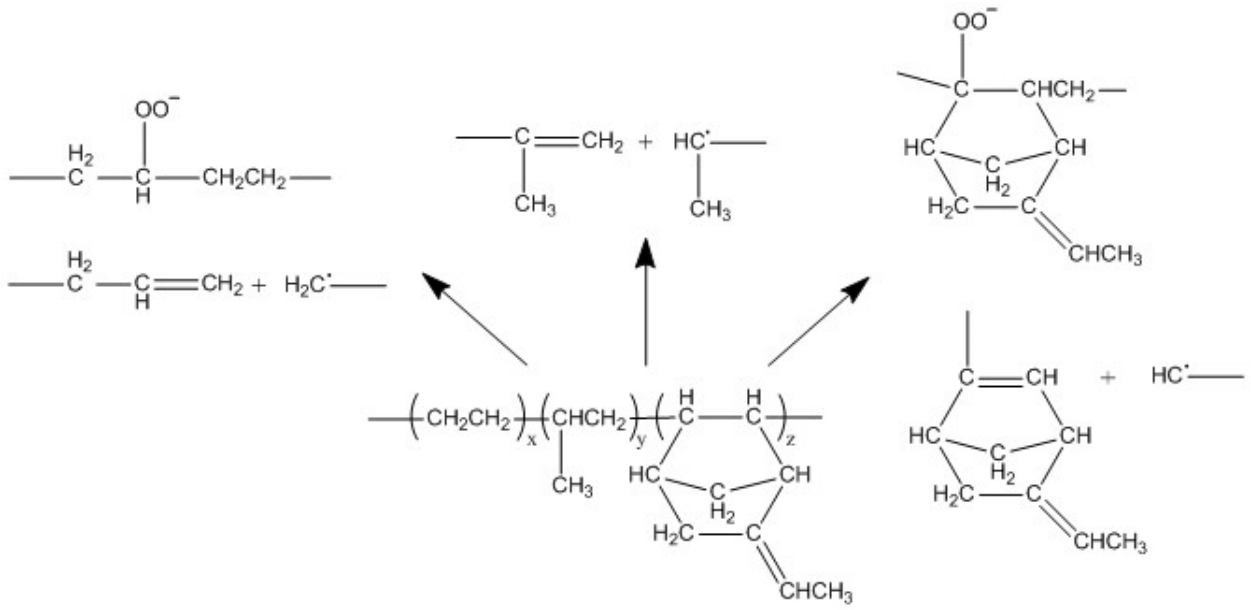

Figure 3. Hypothetical degradation mechanisms of EPDM terpolymer.

3.1.2. Type I FKM

Figure 4 illustrates the ATR-FTIR absorption spectra and the appearance of type I FKM O-rings after exposure to different environments. For the control, all absorption bands, except for three at 3392, 3189, and 1645 cm^{-1} ascribed to water, were related directly to three different fluorocarbon groups [1,21-23], CF (V_{CF}) at 1391 cm^{-1}, CF_2 asymmetric ($V_{as\ CF2}$) at 1211, and CF_2 symmetric ($V_{s\ CF2}$) at 1134 cm^{-1}, and CF_3 at 877 cm^{-1}, within the FKM copolymer structure the absorption bands at 2920 and 2852 cm^{-1} were the C-H ($V_{as\ C\text{-}H}$), and ($V_{s\ C\text{-}H}$) stretching modes in VDF. After exposure to No. 1 and 2 environments, the appearance of both O-rings remained unchanged. However, there were two major changes in spectral features under the No. 1 environment: first, the peak intensity of C-H bands declined considerably, and two new bands emerged at 1716 and 1608 cm^{-1}. Possible contributors to these new bands are the C=O ($V_{C=O}$) [21] stretching at 1716 cm^{-1}, and C=C ($V_{C=C}$) at 1608 cm^{-1} representing the oxidation of VDF. The C-H peak was undetectable in the spectra of the sample exposed in the No. 2 aerated steam environment, suggesting a higher level of Type I FKM oxidation in aerated than in non-aerated steam. On the other hand, there were no remarkable changes in the peak intensity of all the fluorocarbon-related bands compared with that of the control.

Unlike the steam environments, the drilling and geo-brine fluids visibly degraded this material. As seen in photographs, the O-rings had multiple cracks, partial tears, breakage, surface spalling, and severe deposition of scales (Figure 4d and 4e).

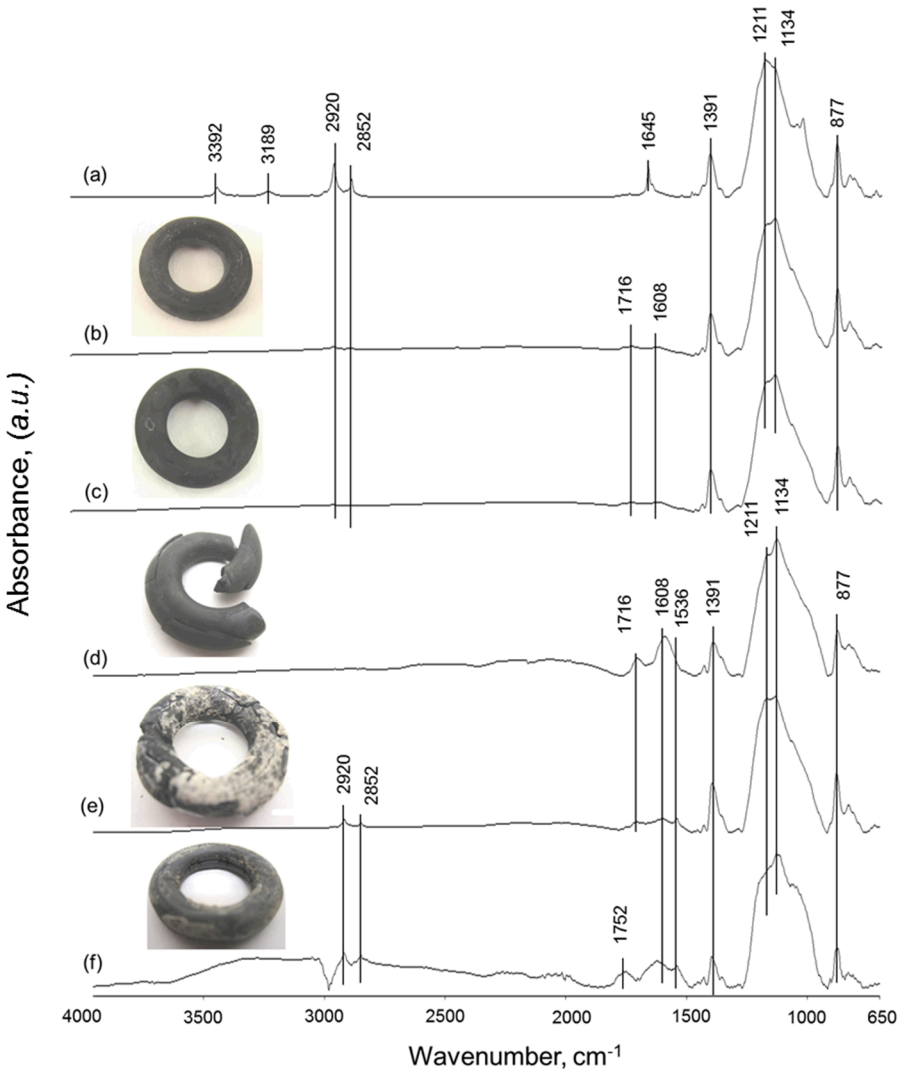

Figure 4. ATR-FTIR absorption spectra and appearance for Type I FKM O-rings before (a) control, and after**:** (b) No. 1 non-aerated (N_2), (c) No. 2 aerated steam/cooling cycles, (d) No. 3 drilling fluid, (e) No. 4 geo-brine fluid, (f) No. 5 thermal shock tests.

The ATR-FTIR survey on oxidation derivatives formed in these degraded O-rings showed the following: three derivatives, C=O ($V_{C=O}$) at 1716 cm^{-1}, C=C ($V_{C=C}$) at 1608 cm^{-1} [24,25], and COO^-, asymmetric ($V_{as\ COO^-}$), at 1536 cm^{-1}, were incorporated into type I FKM structure, and the C-H-related band intensities at 2920 and 2852 cm^{-1} were very weak. In contrast, the appearance of the No. 5-exposed O-ring was far better, strongly suggesting that type I FKM copolymer is more resistant to thermal shock than to drilling and geo-brine fluids. However, three oxidation derivatives, C=C, COO^-, and COOH (V_{COOH}) at 1752 cm^{-1} [1] were evident in this sample along with decayed intensity of C-H bands.

This data, in conjunction with previous studies [4, 6, 22, 24, 26, 27], suggest that the poly-VDF in type I FKM was oxidized preferentially over poly-HFP (Figure 5). Similarly to EPDM, type I

FKM oxidation depended on the exposure environment. The material was affected by the chemical ingredients present in the drilling fluid and the geo-brine fluid, but unaffected by the D.I. water used in the aerated- and non-aerated-steam, or by thermal shock. Thus, the oxidation due to the combination of hydrothermal and chemical effects was detrimental to the integrity of O-rings.

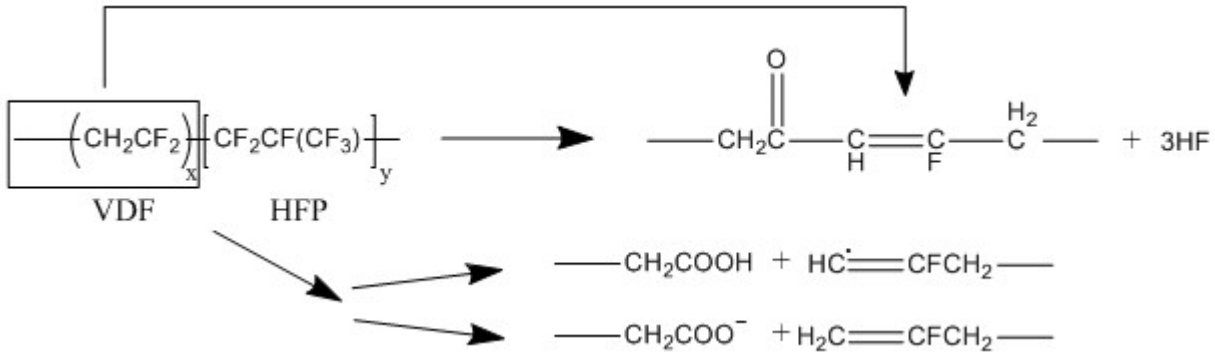

Figure 5. Degradation mechanism of type I FKM copolymer.

3.1.3. Type II FKM

Figure 6 shows the ATR-FTIR spectra and the appearance of type II FKM O-rings after exposure in the five environments. Since the structure of the type II FKM terpolymer, poly(VDF)-*co*-(HFP)-*co*-(TFE), resembles that of the type I but incorporates an additional poly-TFE fluorocarbon, the spectral features of the type I and type II controls are similar. The spectrum included four fluorocarbon-related bands, CF (V_{CF}) at 1391 cm^{-1}, CF_2 asymmetric ($V_{as\ CF2}$) at 1114 cm^{-1}, and CF_2 symmetric ($V_{s\ CF2}$) at 1030 cm^{-1}, and CF_3 at 878 cm^{-1}, and two hydrocarbon-related bands, C-H ($V_{as\ C\text{-}H}$), and ($V_{s\ C\text{-}H}$) at 2920 and 2852 cm^{-1}. Of particular notice in the spectral features was the very weak intensity of the $V_{as\ C\text{-}H}$ and $V_{s\ C\text{-}H}$ bands, compared with that of type I; in fact, the value of $V_{as\ C\text{-}H}$ / $V_{as\ CF2}$ absorbance height ratio in type II was nearly ten-fold lower than that of type I (0.0349 versus 0.342). Based on the differences in this ratio Type II appeared to have a lower proportion of poly-VDF to other poly-fluorocarbons than Type I. Although there were no significant changes in physical appearance, type II also suffered from oxidation after exposure in No. 1 and 2 environments. Like type I, the oxidation derivatives were identified as containing C=O ($V_{C=O}$) at 1719 cm^{-1}, and C=C ($V_{C=C}$) at 1602 cm^{-1}. Furthermore, the C-H bands vanished after exposure in aerated steam/ testing.

The O-ring exposure to drilling fluid resulted in multiple cracks and partial tearing and spalling. However, the polymer resistance to geo-brine and thermal shock tests was better, relative to type I, since the O-rings did not show any cracking or tearing after these tests. As expected, all O-ring samples were oxidized, and the oxidation derivatives contained C=O, C=C, COOH, and COO^- groups. No C-H-related bands were detected in the samples exposed to the drilling fluid and thermal shock.

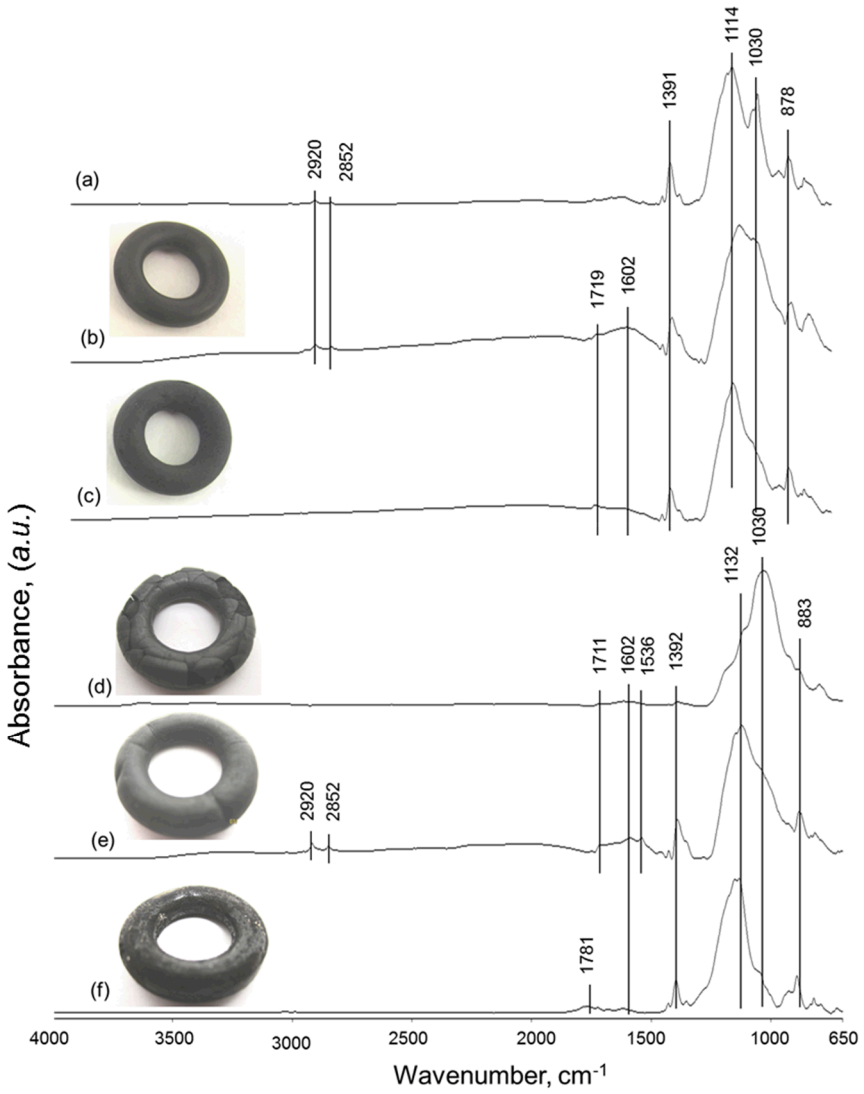

Figure 6. ATR-FTIR absorption spectra and appearance for Type II FKM O-rings before (a) control, and after**:** (b) No. 1 non-aerated (N_2), (c) No. 2 aerated steam/cooling cycles, (d) No. 3 drilling fluid, (e) No. 4 geo-brine fluid, (f) No. 5 thermal shock tests.

The list of the different tested environments in the order from the most damaging to the least damaging was similar for both type I and type II FKM: drilling fluid > aerated steam/cooling ~thermal shock ~ geo-brine fluid > non-aerated steam/cooling. This fact suggests a similar oxidation mechanism for both types of FKM, namely, preferential oxidation of poly- VDF. Since type II contains a lower proportion of poly- VDF it was more stable in the test environments than type I.

3.1.4. FEPM

Figure 7 gives the ATR-FTIR spectra and the appearance for FEPM O-rings after exposure to No. 1 to No. 5 environments. Since FEPM is the copolymer consisting of poly(TFE-*co*-P), the

spectrum of the control revealed the C-H asymmetric ($V_{as\ C\text{-}H}$), and symmetric ($V_{s\ C\text{-}H}$) absorption bands at 2920 and 2852 cm^{-1}, respectively, the CH_2- scissoring (δ_{CH2}) in region of 1465-1442 cm^{-1}, the C-H bending vibration (δ_{CH}) at 1388 cm^{-1}, CF (V_{CF}) at 1326 cm^{-1}, and CF_2 ($V_{as\ CF2}$) at 1168 and CF_2 ($V_{s\ CF2}$) in region of 1089-1014 cm^{-1}. The band at 1688 cm^{-1} may be due to water. There was no significant change in spectral features of the O-ring exposed to the No. 1 environment, except for the incorporation of one new band at 1564 cm^{-1} attributed to the COO^-, asymmetric stretching ($V_{as\ COO^-}$).

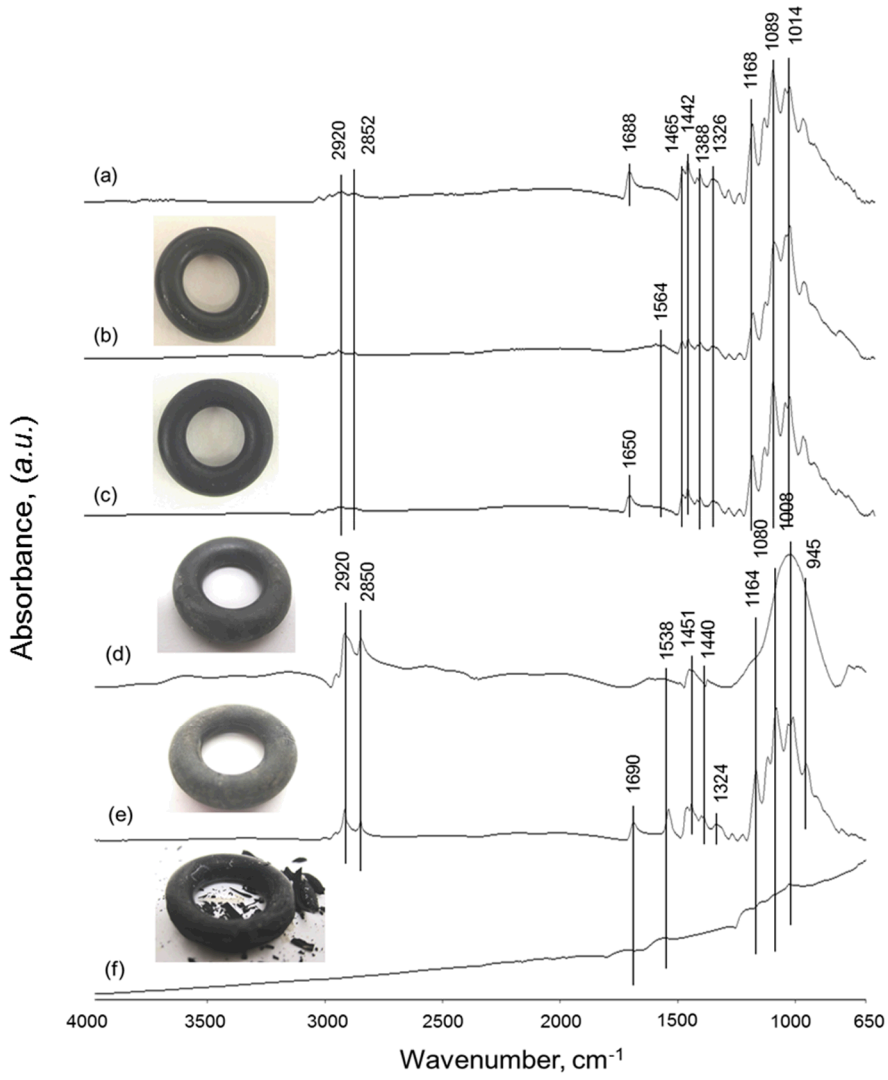

Figure 7. ATR-FTIR absorption spectra and appearance for FEPM O-rings before (a) control, and after**:** (b) No. 1 non-aerated (N_2), (c) No. 2 aerated steam/cooling cycles, (d) No. 3 drilling fluid, (e) No. 4 geo-brine fluid, (f) No. 5 thermal shock tests.

After exposure in No. 2 environment, another additional band appeared at 1650 cm^{-1} attributed to C=C ($V_{C=C}$). The spectra of O-rings tested in No. 3 and 4 environments showed formation of oxidation derivatives with groups like the C=O and COO^-; however, the strong absorption bands of all TFE- and propylene-associated groups were still present indicating relatively good integrity of the O-ring after exposure to drilling and geo-brine fluids. Further, there was no silicate-related band, suggesting that although the surface of O-ring was oxidized, it seemed to resist the deposition of silicate scales. On the other hand the thermal shock testing (environment No. 5) considerably diminished the integrity of O-ring leading to local tearing and partial spalling. Correspondingly, the spectrum revealed the disappearance of all C-H- and CH_2-related bands, considerable reduction of the intensities of the CF- and CF_2-associated bands, along with the appearance of oxidation-induced derivatives such as C=O ($V_{C=O}$) at 1690 cm^{-1}, and COO^- ($V_{as\ COO^-}$) at 1538 cm^{-1}.

The results demonstrated that FEPM has great stability in hydrothermal and harsh chemical environments; however, one drawback was its vulnerability to the hot dry air heating/water quenching (thermal-shock) environment (No.5).

Based upon two pieces of evidence: 1) the elimination of all C-H- and CH_2-related bands in FEPM, and, 2) the presence of the CF and CF_2 bands after the thermal shock, we concluded that the degradation of FEPM may be initiated at Poly-P unit (Figure 8) [28-30].

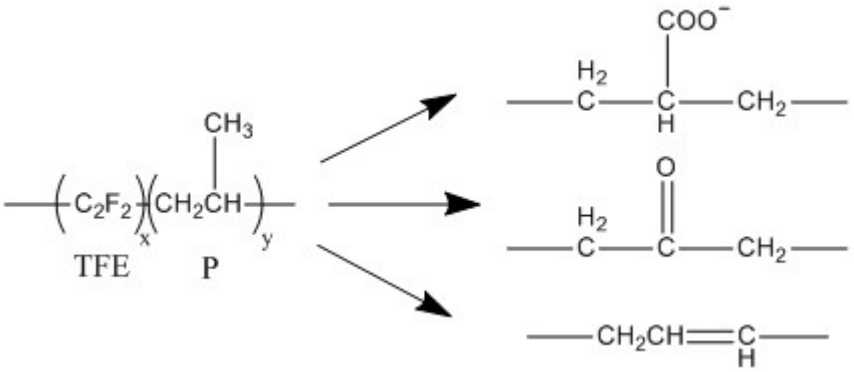

Figure 8. Degradation mechanism of FEPM copolymer.

3.1.5. FFKM

Figure 9 shows the ATR-FTIR spectra in the range between 1700 and 650 cm^{-1}, where the most changes took place and the appearance of FFKM O-rings after exposure to the five environments. The spectrum of the control FFKM, poly(TFE-*co*-PMVE) copolymer structure contained five representative bands at 1287, 1177, 1140, 1095, and 879 cm^{-1}. The contributors to these bands were as follows; CF (V_{CF}) at 1287 cm^{-1}, and CF_2 ($V_{as\ CF2}$) at 1177, and CF_2 ($V_{s\ CF2}$) at

1095 cm^{-1}, CF_3(V_{CF3}) at 879 cm^{-1}, and C-O-C asymmetric ($V_{as\ C\text{-}O\text{-}C}$) and symmetric stretching ($V_{s\ C\text{-}O\text{-}C}$), at 1140 and 1005 cm^{-1}, respectively, as shoulder bands. As is seen in the photographs, the O-rings did not change visually after exposure to the test environments with the exception of a scale deposition in the drilling fluid (Figure 9(e)). Correspondingly, although shifts in some bands were visible, in general, the spectral features were similar to those of the control, and unlike for other O-rings, it was very difficult to identify the presence of oxidation derivatives. A pronounced band that appeared at 1014 cm^{-1} after the exposure to drilling fluid was assigned to the silicate scale. A new band between 1500 and 1600 cm^{-1} was not identified; it could be a result of sample contamination in the oven.

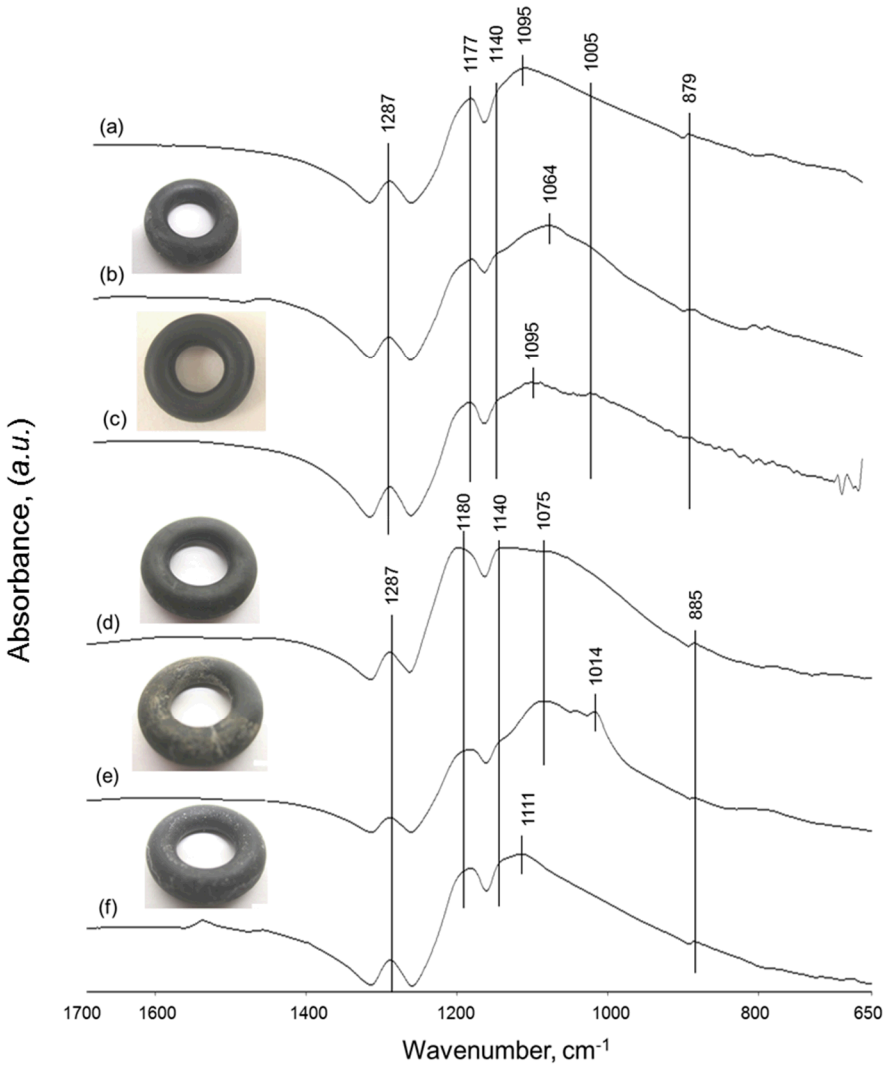

Figure 9. ATR-FTIR absorption spectra and appearance for FFKM O-rings before (a) control, and after**:** (b) No. 1 non-aerated (N_2), (c) No. 2 aerated steam/cooling cycles, (d) No. 3 drilling fluid, (e) No. 4 geo-brine fluid, (f) No. 5 thermal shock tests.

The FFKM O- ring displayed the best performance in these five different harsh environments, compared with all other O-rings made of EPDM, Type I and II FKM, and FEPM.

3.1.6. FSR

Figure 10 shows the ATR-FTIR spectra after exposure to the five environments and the appearance for FSR O-ring after No. 1 environment. The spectrum of the control FSR copolymer, poly(PS-*co*-TFPPS), encompassed eleven major bands: $V_{\text{as CH}}$ and $V_{\text{s C-H}}$ at 2968 and 2918 cm^{-1}, δ_{CH2} at 1447 cm^{-1}, δ_{CH3} at 1370 cm^{-1}, Si-C bending vibration ($\delta_{\text{Si-C}}$) at 1262 and 894 cm^{-1}, Si-C stretching mode ($V_{\text{Si-C}}$) at 794, 767, and 696 cm^{-1}, and Si-O-Si stretching ($V_{\text{Si-O-Si}}$) at 1056 and 1006 cm^{-1} [31-36]. Additionally, the $\delta_{\text{S-C}}$ band at 894 cm^{-1} was likely overlapped by the V_{CF3} band.

A dramatic change in spectral features was observed from the sample exposed in non-aerated steam; most of the bands, except for an intensive $V_{\text{Si-O-Si}}$ signal and several $V_{\text{Si-C}}$ –related bands, were eliminated, and no oxidation derivatives formed, as a result of severe hydrothermal degradation of FSR. In fact, the O-ring was disintegrated. The result was similar for all tested environments, the O-rings failed in all of them. Several investigators had studied the mechanism of hydrothermal degradation for silicon rubber [37-41]. They reported that three linkages within the FSR structure, $Si\text{-}CH_3$, $–CH_2$, and –O, were vulnerable to rupture. Such bond breakages led to the generation of silanol, Si-OH, groups at the rupture sites and then condensation reactions between silanols created new oxygen-bridged Si-O-Si linkages. Assuming a similar degradation mechanism may occur in FSR, the reason for disappearance of the majority of hydrocarbon-related bands could be the breaking off of $–CH_3$ and $–CH_2$ groups. Furthermore, the development of an intensive Si-O-Si signal is likely associated with an increased number of new Si-O-Si linkages. These new Si-O-Si linkages formed by condensation reactions may be created during the step in which O-rings are heated at 90°C before FT-IR analysis. On the other hand, since the $V_{\text{Si-C}}$ –related bands were directly related to the Si-C bond in $Si\text{-}CH_3$ groups, some $Si\text{-}CH_3$ may be present as the end groups. If this hypothesis is reasonable, the following degradation mechanism of FSR in all hydrothermal-associated geothermal environments at 300°C can be postulated (Figure 11).

3.2. TGA analysis

To support the above information and evaluate changes in the thermal stability of the elastomers after the exposures to the aggressive environments, the thermal degradation of the O-rings was evaluated at temperatures of up to 700°C. The following information was collected: 1) the onset temperature of weight loss, 2) the temperature of the maximum decomposition rate, and 3) the percentage of the total mass loss during the entire thermal decomposition. Figure 12 shows TGA-DTG curves for type I FKM exposed to steam/cooling tests as an example and Table 3

summarizes the information on decomposition temperatures and percent of the total mass loss for different O-ring compositions.

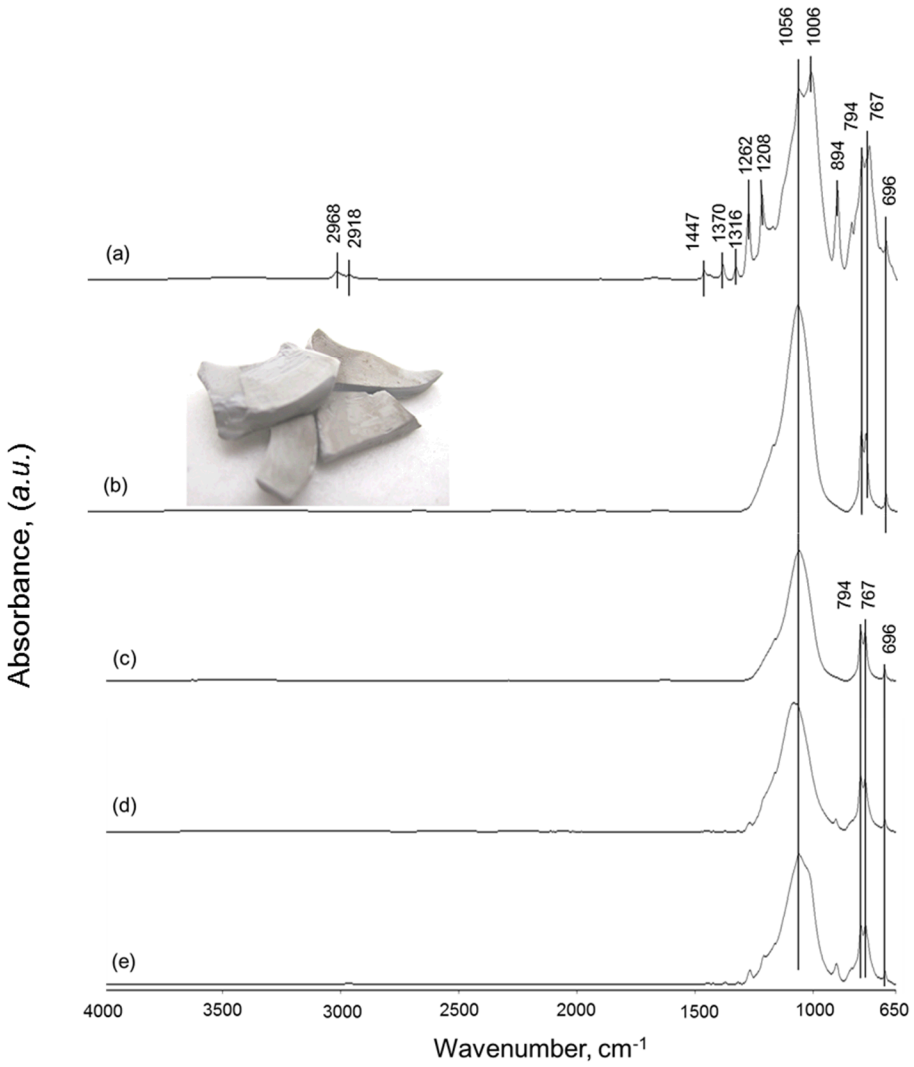

Figure 10. ATR-FTIR absorption spectra and appearance for FSR O-rings (a) control, and after**:** (b) No. 1 non-aerated (N_2), (c) No. 2 aerated steam/cooling cycles, (d) No. 3 drilling fluid, (e) No. 4 geo-brine fluid, (f) No. 5 thermal shock tests.

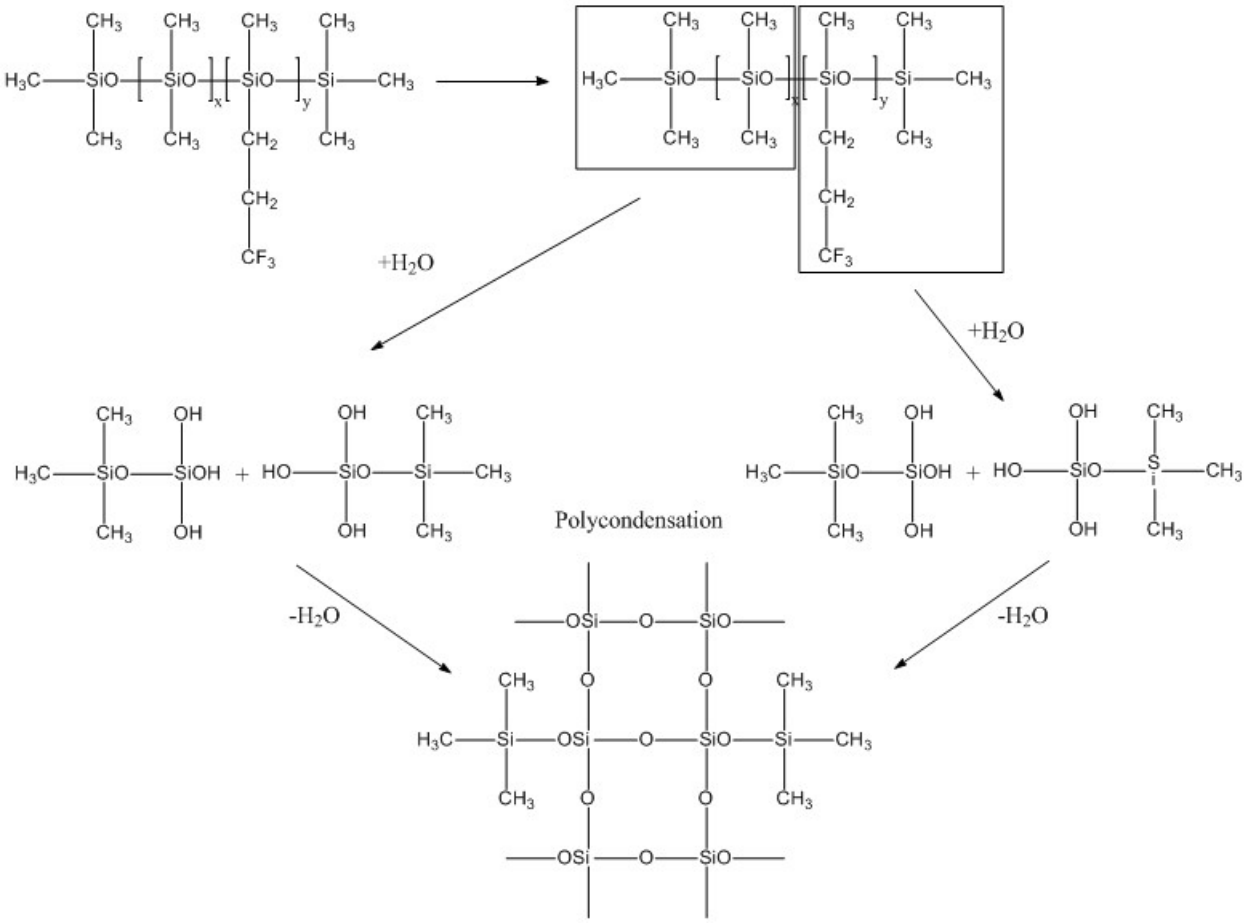

Figure 11. Proposed hydrothermal degradation mechanism of FSR

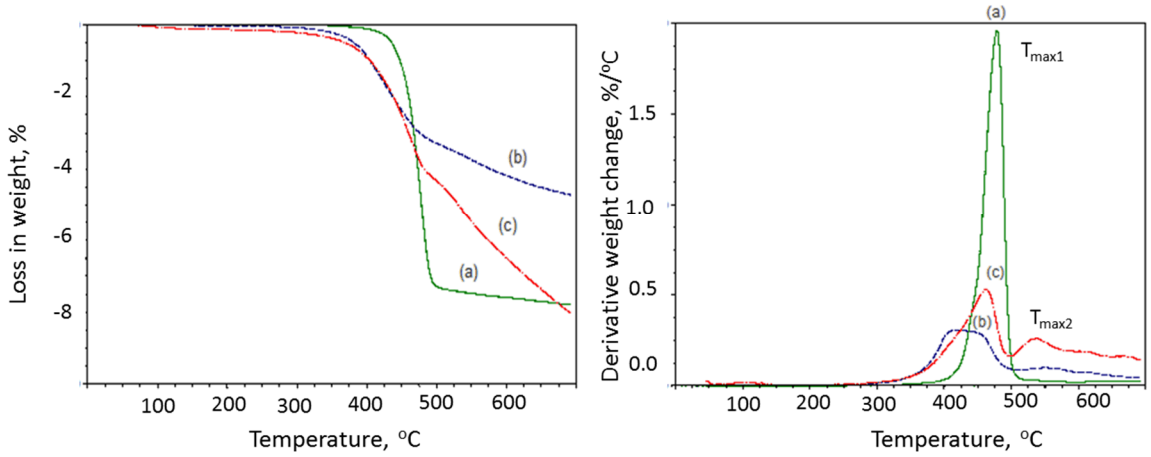

Figure 12. TG (left) and DTG (right) thermograms for type I FKM before (a) and after exposure in (b) No. 1 non-aerated (N_2), and (c) No. 2 aerated steam/cooling cycles environments.

3.2.1. EPDM

Sample changes due to oxidation cause a decrease in the on-set temperature of weight loss for EPDM. Only for the sample exposed to the geo-brine fluid did the onset temperature not decrease. Its thermal behavior was similar to that of the control suggesting minor sensitivity of EPDM to this environment. The sample exposed to the thermal shock environment had the lowest decomposition onset temperature of only 29°C (vs. 118°C for the control). The TGA of this sample showed a low-rate mass loss up to 700°C typical of oxidized carbonaceous compounds. This result is in agreement with the FT-IR spectrum free of C-H bonds, indicating strong sample oxidation. In the case of non-aerated and aerated steam environments the onset temperature decrease was accompanied by the reduction in the percent of the total mass loss likely caused by the formation of oxidation derivatives along with the scission of hydrocarbon backbone chains within the EPDM structure. According to the literature [14] these derivatives convert into carbonaceous by-products that lead to the decrease of the total mass loss.

The sample exposed to the drilling-fluid (environment No. 3) had a maximum rate of thermal decomposition at higher temperature than the control and lost higher percentage of its weight (514°C vs. 476°C and 3.62 % vs. 2.86 % respectively). These changes may be due to the interactions between the EPDM and the drilling fluid. No further work was done on identification of these products.

There is a general agreement between the FT-IR and TGA measurements, showing major changes in the thermal-shock exposed sample and limited alterations in the samples exposed to geo-brine and drilling fluids.

Based upon two factors, 1) material stability after the exposures as determined from decomposition onset and maximum rate temperatures (T_o and T_{max}), and 2) the % of the total weight loss (*TWL)* values, the stability of the EPDM O-rings to the test environments in the order of the most to the least stable is as follows: No. 3 drilling fluid > No. 4 geo-brine fluid > No. 1 non-aerated steam/cooling > No. 2 aerated steam/cooling >> No. 5 thermal shock.

Table 3. The temperatures of the onset of the weight loss ($T_{o)}$, of the maximum decomposition rate ($T_{max)}$, and % of Total Weight Lost *(TWL)* values for O-rings before and after exposure in different environments

Testing environment	T_o, °C	$T_{max.}$, °C	*TWL,* weight %
EPDM			
Control	118	476	2.86
No. 1 non-aerated steam	94	467	2.65
No. 2 aerated steam	44	458	2.45
No. 3 drilling fluid	95	514	3.62
No. 4 geo-brine fluid	117	474	2.72
No. 5 thermal shock	29	-	-
Type I FKM			
Control	300	478	3.52
No. 1 non-aerated steam	74	425 (533)*	1.14 (1.1; 0.04)**

No. 2 aerated steam	50	462 (539)*	1.42 (1.13; 0.28)**
No. 3 drilling fluid	197	455	1.83
No. 4 geo-brine fluid	68	469 (169)*	1.85 (1.82; 0.03)**
No. 5 thermal shock	286	479	2.21
Type II FKM			
Control	228	497	3.39
No. 1 non-aerated steam	65	484	2.27
No. 2 aerated steam/	53	484	1.85
No. 3 drilling fluid	54	465	1.09
No. 4 geo-brine fluid	107	469	1.85
No. 5 thermal shock	241	492	2.93
FEPM			
Control	152	514	3.64
No. 1 non-aerated steam	54	506	3.35
No. 2 aerated steam	47	502	3.25
No. 3 drilling fluid	114	480	2.83
No. 4 geo-brine fluid	95	513	3.66
No. 5 thermal shock	27	507	0.65
FFKM			
Control	354	478	3.58
No. 1 non-aerated steam	273	483	3.58
No. 2 aerated steam	162	478	3.59
No. 3 drilling fluid	229	494	3.53
No. 4 geo-brine fluid	141	478	3.52
No. 5 thermal shock	372	487	3.66
FSR			
Control	168	522	2.43
No. 1 non-aerated steam	51	-	-
No. 2 aerated steam	-	-	-
No. 3 drilling fluid	40	422	0.009
No. 4 geo-brine fluid	41	563	0.30
No. 5 thermal shock	49	498	0.91

* - temperature of the second decomposition rate peak; **- mass loss rates of the first and the second peaks are given in parenthesis

3.2.2. Type I FKM

All test environments caused a decrease in the thermal stability of this elastomer as evidenced by the reduction in decomposition onset temperature. This stability decrease was minimal for the thermal-shock tested sample (environment No. 5) and maximal for the aerated steam (environment No. 2). The DTG curves clearly showed formation of some oxidation derivatives that gave second decomposition peaks for samples treated under both steam conditions (Table 3 and Figure 12) and in geo-brine fluid (Table 3), while the control sample decomposed in a single step. The total mass losses decreased in comparison with the control sample for all the

environments suggesting formation of oxidized carbonaceous derivatives as a result of FKM oxidation. It is difficult to rank type I FKM stability in different environments based on the TGA-DTG data. The sample seemed to be more vulnerable to steam tests and geo-brine fluid than to drilling fluid. The thermal shock testing had the least impact on type I FKM elastomer. FT-IR measurements showed minimal formation of oxidation derivatives as well as the decay of the CH band after the thermal shock, bond degradation, and oxidation after exposure in the drilling and geo-brine fluids, which support these conclusions.

3.2.3. Type II FKM

Unlike type I FKM all type II FKM samples decomposed in a single step (Table 3). The decomposition onset temperatures significantly decreased for samples tested under the steam conditions (more than 150°C reduction) and in geo-brine fluid (more than 100°C reduction) indicating the strong effect of these environments on the elastomer. On the other hand, the thermal shock environment did not affect the elastomer's decomposition temperature. The DTG data showed wide decomposition peaks for O-rings treated in drilling and geo-brine fluids (data not shown) suggesting formation of oxidation derivatives with varied decomposition temperatures. The decrease in total weight losses indicates formation of carbonaceous products as in the case of EPDM and type I FKM elastomers.
Data comparison with the type I FKM shows that the type II elastomer was less susceptible to both aerated and non-aerated steam conditions since its total weight losses decreased only by 32% against 68% for type I FKM for non-aerated environment and by 45% against 60% respectively for the aerated one implying a smaller amount of carbonaceous oxidation products in the case of type II FKM. Accordingly, the FT-IR data showed that although all Type II FKM O-ring samples were oxidized, they were less susceptible to the harsh environments than Type I FKM.

Based upon the overall data the stability of type II FKM O-rings in the tested environments ordered from the most to the least stable is: No. 5 thermal shock > No. 1 non-aerated steam/cooling > No. 2 aerated steam/cooling > No. 4 geo-brine fluid > No. 3 drilling fluid.

3.2.4. FEPM

FEPM O-rings showed single-step decomposition curves after all test environments (Table 3). These O-rings were sensitive to both steam environments and highly sensitive to the thermal-shock tests. On the other hand this elastomer was only mildly sensitive to the drilling fluid and even less so to the geo-brine fluid. This is in agreement with the FT-IR data that indicated relatively good integrity of this elastomer after exposure to drilling and geo-brine fluids but a high sensitivity to thermal shock. From these data the stability of FEPM in the tested environments, ordered from the highest to the lowest, is: No. 4 geo-brine fluid > No. 1 non-

aerated steam/cooling > No. 2 aerated steam/cooling > No. 3 drilling fluid >> No. 5 thermal shock.

3.2.5. FFKM

There was a slight decrease in the temperatures of the decomposition onset for the FFKM O-rings after exposure to No.1-4 environments; however, the total weight losses and the decomposition temperature ranges did not change significantly. In agreement with the FT-IR data the results suggest only a mild effect of the aggressive environments on the FFKM elastomer and its high resistance to the thermal shock tests (Table 3).

3.2.6. FSR

As described earlier in ATR-FTIR study, all the environments severely degraded the FSR O-ring. Among all the employed elastomeric polymers, the "as-received" FSR was identified as O-ring possessing the highest T_{max} value of 522°C (Table 3). However, its undesirable vulnerability to all hydrothermal environments suggested that it would be very difficult to use this elastomer in geothermal fields. Thus, no further study was done with FSR.

3.3. µEDX imaging and Ca mapping analyses

As previously identified in the ATR-FTIR analysis, the carboxylate, $–COO^-$, group was among the several derivatives formed by the oxidation of the elastomeric polymers. It is possible for the $–COO^-$ group to react with Na, K, Mg, and Ca counter mono- and di-valent cations present in No. 3 and No. 4 environments (drilling and geo-brine fluids). This reaction would engender the formation of a $–COO^-{}^+M$ (M = metal cation) carboxylate salts. Another possible pathway of metal cations permeation into the O-rings is through the reactions with hydrofluoric acid that forms during the degradation of FKM elastomers. To obtain information on the depth of O-ring oxidation and metal cation penetration as a result of reaction with the carboxylate anion or hydrofluoric acid, Ca measurements were carried out by µEDX elemental mapping analysis coupled with micro-imaging. The µEDX analyses were performed on an area of 2.0 x 1.5 mm (3 mm^2). The color-coding of 3.7 keV Kα energy line of calcium was such that the areas with the highest calcium concentration show up in white and red while Ca-free zones are blue.

3.3.1. EPDM

The Ca mapping image of the EPDM samples after drilling and geo-brine fluids closely resembled that of the control. There was no additional calcium in the body of the O-rings in comparison with the control. This result implies that the reaction between carboxyl anion detected in the O-ring by ATR-FTIR analysis and calcium from drilling and geo-brine fluids was

minimal, if any. In fact, the O-ring calcium content slightly decreased in brine probably due to the calcium reacting with the anions in this fluid and leaching out of the O-ring. On the other hand, zinc content increased, possibly due to the metal cation reaction with the carboxylic acid anion (data not shown).

3.3.2. Type I FKM

Figure 13 represents changes in morphologies and the μEDX Ca maps for the cross-sectional area marked with a red rectangle from the edge to the core of type I FKM O-rings before and after exposure in No. 3 drilling- and No. 4 geo-brine fluids. The Ca content of the control was very low (dark and light blue colors).
The mapping of O-rings exposed to the drilling and geo-brine fluids showed Ca permeation through the entire tested area. The amount of the calcium reacted with the O-ring was significantly higher after the exposure to the drilling fluid (white and red colors) than after the geo-brine fluid (green and yellow colors). Since there was no calcium permeation into the body of the EPDM O-ring, where, according to ATR-FTIR measurements, carboxyl presence was more important than in the FKM one, it is reasonable to assume that strong calcium permeation into the type I FKM O-ring was due to the cation reaction with hydrofluoric acid accumulated in the degraded elastomer.

3.3.3. Type II FKM

Figure 14 shows the μEDX maps of Ca for the cross-sectional area marked with a red rectangle from the edge to the core of type II FKM O-rings before and after exposure to the No. 3 (drilling) and No. 4 (geo-brine) environments. The Ca mapping image of the control O-ring showed that the material already contained some Ca, as indicated by the uniform distribution of white- and red-colors throughout the cross-sectional area. For the O-ring exposed to the drilling fluid (No. 3 environment), the morphological image revealed a rim-like layer in the subsurface. Additionally, micro-cracks were observed in the interfacial regions between the rim layer and the rest of the O-ring body, demonstrating that the formation of this rim resulted in structural damage. The Ca mapping image of this defect-laden area revealed a relatively high concentration of Ca, represented by the dense red-color, down to a depth of at least 0.4 mm from the surface. The O-ring exposed to geo-brine (No. 4 environment) also showed a rim layer in the subsurface. However, this layer was thinner than for No. 3 drilling fluid environment, and there were no micro-defects. Correspondingly, the dense red-color is evident in a superficial layer of around 0.2 mm. Thus, the extent of Ca penetration in No. 3 (drilling fluid) appeared to be much higher than in No. 4 (geo-brine fluid), suggesting a higher extent of oxidation. This result is in agreement with the results of the ATR-FTIR and TGA analyses. The creation of the oxidized outer layer is likely the result of diffusion limited oxidation (DLO). DLO occurs when the diffusion rate of oxygen into the material is slower than the oxidation reactions, thus limiting

those reactions to the outermost edges of the material. Similarly to type I FKM, the calcium permeation was possibly a result of the reaction between calcium ions from the fluids and hydrofluoric acid in the body of the degraded O-rings.

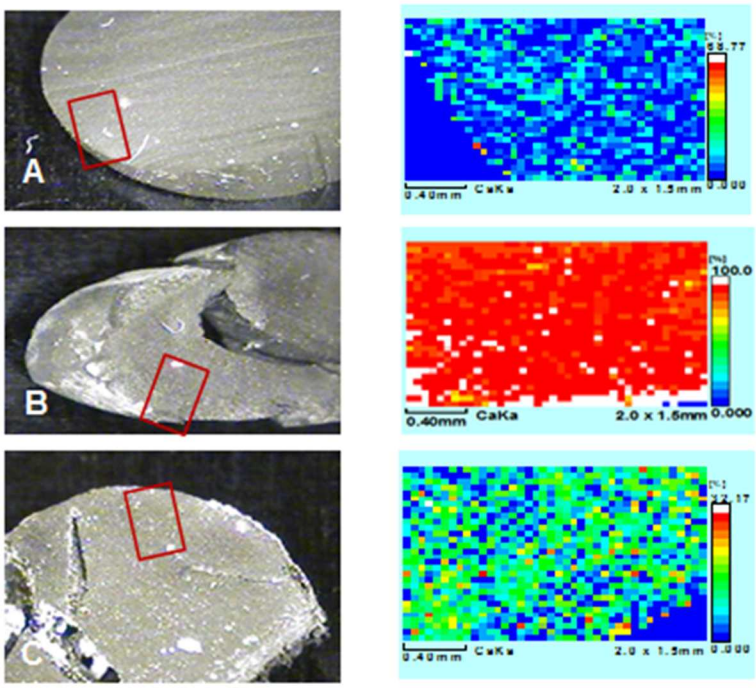

Figure 13. EDX mapping of Ca coupled with micro-structure images for cross-sectional area of type I FKM before (a) and after exposure in (b) No. 3 (drilling fluid), and (c) No. 4 (geo-brine fluid).

3.3.4. FEPM

Similarly to EPDM, the FEPM O-rings exposed to drilling and geo-brine fluids did not have any micro-defects or any significant Ca ion permeation, validating their integrity under those conditions and confirming that there was no any significant reaction between the carboxyl formed during the oxidation of these materials (ATR-FTIR data) and calcium from the aggressive fluids (data not shown). Also similarly to EPDM, zinc content increased and sulfur content decreased after the exposure of this elastomer to the aggressive fluids.

3.3.5. FFKM

The control FFKM O-ring was Ca-free. Similarly, there was no calcium in the O-ring body after No. 3 (not shown) and No. 4 environments (Figure 15), highlighting that Ca ions did not migrate into the material. As expected, there were no micro-defects in these O-rings. One interesting observation was the deposition of some Ca-based scales on the surface of the O-ring exposed to No. 4 (geo-brine fluid), suggesting that the surface of the FFKM copolymer might have

undergone a physicochemical modification during the exposure in this environment. This fact strongly supported the results from the ATR-FTIR study. Such scale deposition should be addressed as a potential drawback of FFKM. Although the elastomer possesses an outstanding stability in all environments, scale may accumulate at longer exposure times.

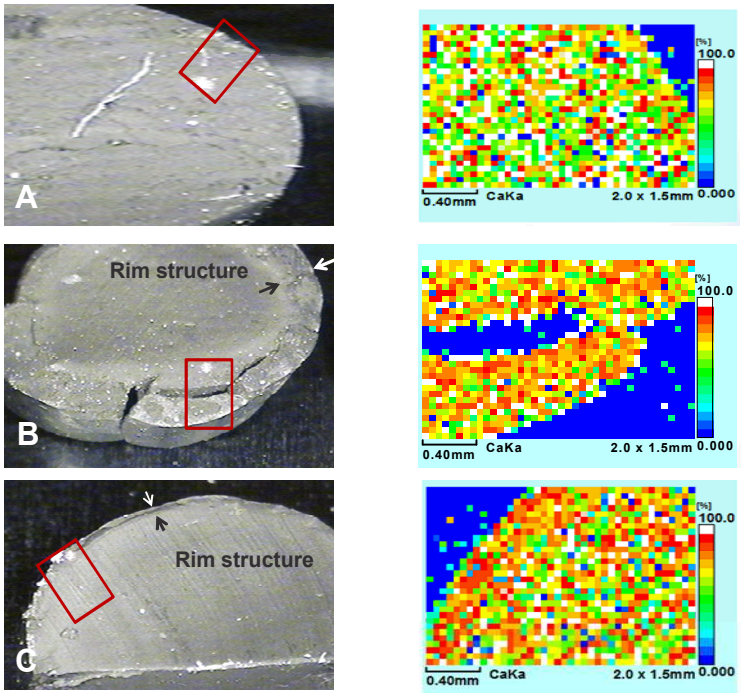

Figure 14. EDX mapping analysis of Ca coupled with images for cross-sectional area of type II FKM before (a), after exposure in (b) No. 3 (drilling fluid), and (c) No. 4 (geo-brine fluid).

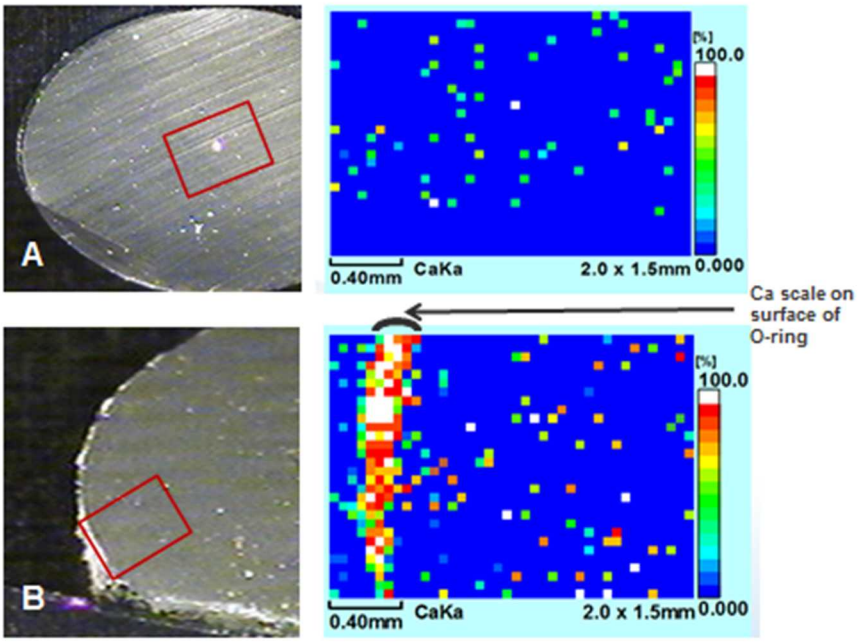

Figure 15. EDX mapping of Ca coupled with micro-structure images for a cross-sectional area of FFKM before (a) and after exposure in (b) No. 4 (geo-brine fluid).

3.4. Modulus Profiling Analysis

Of particular interest in any O-ring application are changes in elasticity, which could negatively impact sealing force (e.g. edge and/or overall hardening or softening). To evaluate such changes after O-ring exposure to different environments an elastic modulus (inverse tensile compliance) was measured on O-ring cross-sections. Figure 16 summarizes results of these measurements for control O-rings and O-rings exposed to the five test environments. The figures show some important discrepancies between modulus measurements at different edges. For the most part these were due to the flaking of the strongly degraded material at edges and, in some cases, due to the uneven scale deposition. Despite these discrepancies the modulus measurements allow the deduction of general tendencies of changes in elastic properties of treated O-rings. An increase in modulus values after a treatment indicates material stiffening while decreased values correspond to material softening.

3.4.1. EPDM

With the exception of geo-brine treatment, all other environments slightly softened the EPDM O-rings (Figure 16a). This softening effect was the strongest after the exposure to the aerated steam/cooling environment. The geo-brine exposure hardened the core of the O-ring. As µEDX measurements showed, the hardening of the material in the geo-brine fluid is not related to the calcium permeation. Reactions with zinc cations from the brine and loss of sulfur cannot be

excluded as contributing factors to this hardening. In general, the changes in the EPDM O-ring elasticity were not dramatic for the tested environments with the exception of the thermal-shock tests, where the O-ring was strongly degraded and therefore not tested.

3.4.2 Type I FKM

The modulus of the control sample for type I FKM was lower than for EPDM suggesting a softer material (1.7 MPa vs. 2.8 MPa for EPDM). The elastomer underwent further softening after exposure to the steam environments and the thermal shock tests (Figure 16b). On the other hand, the O-rings hardened on the edges after all the exposures and throughout the cross sections after the aggressive fluids. According to the results of μEDX measurements, formation of calcium salts (possibly calcium fluoride) could have contributed to the O-ring-body hardening in the drilling and geo-brine fluids. The modulus measurements confirmed that apart from the thermal shock environment, the type I FKM was less resistant to the tests conditions than EPDM.

3.4.3. Type II FKM

The control sample of type II FKM was harder than type I one and had a modulus similar to EPDM (3.0 MPa vs. 2.8 MPa for EPDM) (Figure 16c). The bodies of the O-rings made with this material softened and the edges hardened in all the environments. The softening was the most severe after the thermal shock where the modulus lost almost 80% of its value. The aggressive fluids had the strongest effect on the edge hardening. The sudden drop in modulus at about 0.8 mm distance from the left edge corresponds to the rim structure that damaged the material integrity. In general, in agreement with TGA measurements, the changes in the modulus were less dramatic for type II FKM than for type I. The calcium originally present in type II FKM could have counteracted the effect of hydrofluoric acid release during the degradation of the elastomer through formation of CaF_2.

3.4.4. FEPM

The control FEPM O-ring modulus was more than 4 times higher than for EPDM (14 MPa). There were no dramatic changes in the modulus of the O-ring body after its exposure to the test environments except after the thermal shock tests that resulted in partial O-ring decomposition and hardening of the edges (Figure 16d, blue squares). Note that this sample was smaller in diameter than samples after the other tested environments, which is likely the result of the hardened material flaking off. Some edge softening occurred after the exposures to the geo-brine and steam environments. In general, this material demonstrated good resistance to all but thermal shock test environments.

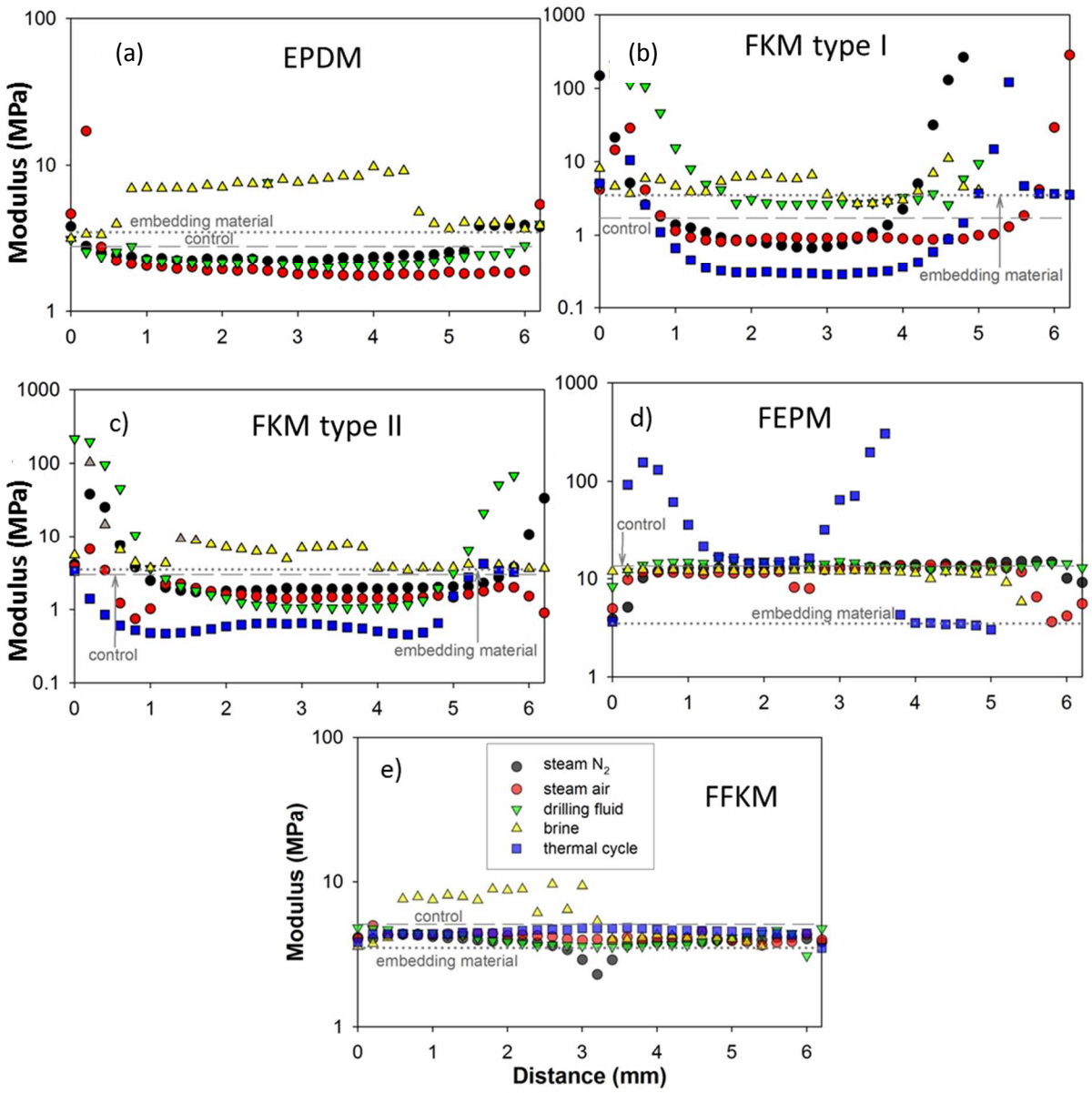

Figure 16. Modulus for cross-sectional areas before and after exposures in test environments for (a) EPDM; (b) FEPM; (c) Type I FKM; (d) Type II FKM; (e) FFKM

3.4.5. FFKM

The FFKM control O-ring had a modulus almost twice as high as EPDM; however, it was almost three times lower than that of FEPM (5.1 MPa for FFKM, 2.8 MPa for EPDM and 14 for FEPM). The changes in the modulus were very small after all the tests for FFKM O-rings (Figure 16e), strongly confirming its excellent resistance to aggressive environments. The higher modulus after the exposure in the drilling fluid at some parts of the elastomer could be a result of the scale deposition, which was also observed in the micro-EDX tests.

4. Summary

O-rings made with six different elastomeric polymers (EPDM, type I- and II-FKM, FEPM, FFKM, and FSR, were exposed in five different environments at 300°C: 1) Non-aerated steam/cooling cycles, 2) aerated steam/cooling cycles, 3) drilling fluid with pH 9-10, 4) CO_2-rich geo-brine fluid with pH 4-5, and 5) thermal-shock cycles. The general sensitivity of the tested materials to the various environments depended largely on the environment itself, in addition to the material composition and structure, which determined the decomposition mechanisms. The following conclusions were drawn from the post-test analyses:

1. In the test environments the hydrocarbon bonds underwent oxidation with the formation of (C=C)- and (COO^-)-containing derivatives. Elastomers with high number of these bonds, such as EPDM and FEPM, were highly sensitive to the environment of heat-quenching thermal-shock tests. On the other hand, these elastomers performed reasonably well in chemically aggressive environments such as drilling- and geo-brine fluids. The micro-EDX tests did not show any calcium permeation into the O-ring bodies from these fluids, implying that there was not any significant reaction between the oxidation derivatives, such as the carboxylic anion and the cations from the fluids. As a result, the mechanical properties of EPDM and FEPM, evaluated by measuring changes in O-rings elasticity, were not strongly affected by the drilling and geo-brine fluids, while significant hardening was observed for the FEPM O-rings and strong decomposition for EPDM O-rings exposed to the thermal shock tests.

2. Elastomers with fluoro-substituted hydrocarbons in their structures, such as hexafluoropropylene (HFP) in type I FKM and HFP and tetrafluroethylene (TFE) in type II FKM, were much more resistant to thermal-shock environment than elastomers rich in hydrocarbons. However, they were more sensitive to the aggressive drilling and geo-brine fluids, where calcium cations from these fluids permeated into the O-rings. One may argue that in aggressive fluids HF in the polymers may have reacted with calcium cations forming solid CaF_2 that caused material hardening. The hardening would be the most severe for the O-rings with the highest content of HFP moieties that form HF during the oxidation (type I FKM) and in fluids with high Ca concentrations. This was the case for type I FKM after the brine exposure. Type II FKM, having lower HFP content, would produce smaller amounts of HF and experience a lesser calcium permeation. In the absence of calcium ions to react with the HF, released as a result of the polymer degradation, the HF could cause a further degradation of the elastomer.

Observations of the significant hardening throughout the O-ring and its partial disintegration (type I FKM) or important edge-hardening (type II FKM) in aggressive fluids with calcium cations and softening in the main body of the O-rings in all other cases support this argument.

3. The FFKM elastomer, which contained only fluorocarbon bonds, ,was the most resistant to all tested environments. Its only shortcoming was the deposition of a silica-related scale after the exposure to geo-brine fluid, possibly due to a surface modification in this aggressive environment.

4. The fluorosilicone chemistry (FSR) was vulnerable to all tested environments resulting in the O-ring disintegration. This elastomeric material is not suitable for geothermal applications.

5. Conclusions

Based upon this study, the stability of various elastomeric materials was ranked from the best "1" to the worst "6" (Table 4). Also, to assess the relation between cost-effectiveness and performance of these O-rings, the raw material costs were compared to that of the most economical, EPDM. As is evident from the table the performances of EPDM and FEPM were very similar, namely, these elastomers were relatively resistant to steam/cooling, drilling and geo-brine fluids and vulnerable to thermal-shock test conditions. The FKM elastomers performed poorly in all environments except under the thermal-shock, while FFKM elastomer O-rings performed well under all test conditions. The FSR O-rings disintegrated in all environments.

One important consideration is the economic impact of elastomeric materials on the end-use products. Therefore, if a cost-effective material possesses a long life-cycle in 300°C hydrothermal and other high temperature environments containing oxidation-promoting chemical ingredients, the products made with this material will have a substantial reduction in total downtime costs due to O-ring failure or replacement, including: strip-down, repair time, material replacement, and installation in the field, consequently reducing the expense of operating and maintaining wells and power plants. Under these considerations, the ideal cost-effective and high-performance elastomeric materials of the future will be required to possess properties bridging the gap between the expensive FFKM, and the less expensive EPDM, both of which showed promising stability under many of the test conditions.

Table 4. Stability ranking of different polymer O-rings (1 being the best) and cost comparison of their raw materials based upon EPDM as the benchmark.

Elastomeric polymer (raw material cost factor based on EPDM)	Non-aerated steam	Aerated steam	Drilling fluid	CO_2-rich geo-brine fluid	Heat-quenching thermal shock
EPDM (1)	2	3	2	3	4
Type I FKM (x2.5)	4	5	5	5	3
Type II FKM (x2.6)	3	4	4	4	2
FEPM (x5.6)	2	2	3	2	4
FFKM (x13.8)	1	1	1	1	1
FSR (x6.3)	5	6	6	6	5

Acknowledgements

This publication was based on the work supported by the Geothermal Technologies Office in the US Department of Energy (DOE) Office of Energy Efficiency and Renewable Energy (EERE), under the auspices of the US DOE, Washington, DC, under Contract No. DE-AC02-98CH 10886.

Sandia National Laboratories is a multi-program laboratory managed and operated by Sandia Corporation, a wholly owned subsidiary of Lockheed Martin Corporation, for the U.S. Department of Energy's National Nuclear Security Administration under contract DE-AC04-94AL85000. We would like to thank Nicholas Giron and Douglas Brunson for their assistance in preparing samples for modulus profiling tests.

References

1. T. Sugama, Surface analyses of fluoroelastomer bearings exposed to geothermal environments, Material Letters 50 (2001) 66-72.

2. A.M. Kader and A.K. Bhowmick, Thermal ageing, degradation and swelling of acrylate rubber, fluororubber and their blends containing polyfunctional acrylates, Polymer Degradation and Stability 79 (2003) 283-295.

3. I. Banik, A.K. Bhowmick, S.V. Raghavan, A.B. Majali, V.K. Tikku, Thermal degradation studies of electron beam cured terpolymeric fluorocarbon rubber. Polymer Degradation and Stability 63 (1999) 413-421.

4. T. Sugama and B. Sullivan, Hydrothermal oxidation of fluoroelastomer bearings after a year-long exposure to geothermal environments, Journal of Materials Science Letters 20 (2001) 1737-1740.

5. H.J. Harwood, Ethylene Diene monomer (EPDM) and Fluorocarbon (FKM) elastomers in the geothermal environment, Journal of Testing and Evaluation 11 (1983) 289-298.

6. S. Mittra, A. Chanbari-Siahkali, P. Kingshott, K. Almdal, H.K. Rehmeier, A. G. Christensen, Chemical degradation of fluoroelastomer in an alkaline environment, 83 (2004) 195-206.

7. R. Fuller, Advanced polymer architecture sealing solutions for oil and gas applications, Sealing Technology, September 2006, 6-11.

8. W. Stahl, Choosing the right elastomers for the right application, World Pumps, October 2006, 30-33.

9. FFKM seals are resistant to chemicals and high temperatures, Sealing Technology, February 2014, 2-3, Parker Hannifin Corp.

10. P. Sui and S. Anderle, Elastomers in drilling fields, Wear 271 (2011) 2466-2470.

11. J. Walters, S. Thorhallsson, and E. Wood, International partnership for geothermal technology zonal isolation for geothermal wells, Working Group Documents, August, 2012.

12. K.T. Gillen, R.L. Clough, C.A. Quintana, Modulus Profiling of Polymers, Polymer Degradation and Stability 17 (1987) 31-47.

13. Q. Zhao, X. Li, and J. Gao, Surface degradation of ethylene-propylene-diene monomer (EPDM) containing 5-ethylidene-2-norbornene (ENB) as diene in artificial weathering environment, Polymer Degradation and Stability 93 (2008) 692-699.

14. G. Tang, Y. Hu, and L. Song, Study on the flammability and thermal degradation of a novel intumescent flame retardant EPDM composite, Procedia Engineering 62 (2013) 371-376.

15. Y. Bao, J. Ma, and Li Na, Synthesis and swelling behaviors of sodium carboxymethyl cellulose-g-poly(AA-co-AM-co-AMPS)/MMT superabsorbent hydrogel, Carbohydrate Polymers 84 (2011) 76-82.

16. S. Mishar, GU. Rani, and G. Sen, Microwave initiated synthesis and application of polyacrylic acid grafted carboxymethyl cellulose, Carbohydrate Polymers 87 (2012) 2255-2262.

17. T. Sugama, T. Pyatina, and A. Muraca, Role of PVA flakes in promoting self-degradation of sodium metasilicate-activated cement under a hydrothermal environment at ≥150°C, J. Technology Innovations in Renewable Energy 2 (2013) 352-365.

18. T. Nakamura, O. Chaikumpollert, Y. Yamamoto, Y. Ohtake, and S. Kawahara, Degradation of EPDM seal used for water supplying system, Polymer Degradation and Stability 96 (2011) 1236-1241.

19. A. Demirbas, A. Sari, and O. Isildak, Adsorption thermodynamics of stearic acid onto bentonite, Journal of Hazardous Materials B135 (2006) 226-231.

20. L. Zhirong, M.A. Uddin, and S. Zhanxue, FT-IR and XRD analysis of natural Na-bentonite and Cu(II)-loaded Na-bentonite, Spectrochmica Acta Part A 79 (2011) 1013-1016.

21. S.J. Lim, K.K. Gleason, D.J. Edell, and E.F. Gleason, Flexible fluorocarbon wire coatings by pulsed plasma enhanced chemical vapor deposition, Journal Vacuum Science Technology A 15 (1997) 1814-1818.

22. S. Mitra, A. Ghanbari-Siahkalia, P. Kingshotta, K. Almdala, H.K. Rehmeierb, and A. G. Christensenc, Chemical degradation of fluoroelastomer in an alkaline environment, Polymer Degradation and Stability 83 (2004) 195-206.

23. C. Biloiu, I. A. Biloiu, Y. Sakai, Y. Suda, and A. Ohta, Amorphous fluorocarbon polymer (a-C:F) films obtained by plasma enhanced chemical vapor deposition from perfluoro-octane (C_8F_{18}) vapor I: Deposition, morphology, structure and chemical properties, Journal Vacuum Science Technology A 22 (2004) 13-19.

24. A.N. Theodore, M. Zinbo, and R.O. Carter III, Characterization of fluoroelastomer networks: II. SEC, FTIR, and ODR analysis, Journal of Applied Polymer Science 61 (1996) 2065-2073.

25. I. Banik, A. K. Bhowmick, S.V. Raghavan, A.B. Majali, and V.K. Tikku, Thermal degradation studies of electron beam cured terpolymeric fluorocarbon rubber, Polymer Degradation and Stability 63 (1999) 413-421.

26. G.J. Knight and W.W. Wright, The thermal degradation of some fluorine-containing elastomers, Thermochimica Acta 60 (1983) 187-194.

27. G.J. Ross, J.F. Watts, M.P. Hill, and P. Morrissey, Surface modification of poly(vinylidene fluoride) by alkaline treatment 1. The degradation mechanism, Polymer 41 (2000) 1685-1696.

28. M. Celina and G.A. George, A heterogeneous model for the thermal oxidation of solid polypropylene from chemiluminescence analysis, Polymer Degradation and Stability 40 (1993) 323-335.

29. S. Morlat, B. Mailhot, D. Gonzalez, and J.L. Gardette, Photo-oxidation of polypropylene/montomorillonite nanocomposites. 1. Influence of naoclay and compatibilizing agent, Chemistry of Materials 16 (2004) 377-383.

30. P. Concepcion, P. Botella, and J.M. Lopez Nieto, Catalytic and FT-IR study on the reaction pathway for oxidation of propane and propylene on V-or Mo-V-based catalysts, Applied Catalysis: A General 278 (2004) 45-56.

31. M. Ouyang, R.J. Muisener, A. Boulares, and J.T. Koberstein, UV-ozone induced growth of a SiO_2 surface layer on a cross-linked polysiloxane film: characterization and gas separation properties, Journal of Membrane Science 177 (2000) 177-187.

32. M. Zou, S. Wand, Z. Zhang, and X. Ge, Preparation and characterization of polysiloxane-poly(butylacrylate-styrene) composite lattices and their film properties, European Polymer Journal 41 (2005) 2602-2613.

33. L. Su, S. Pei, L.L. Hong Li, Y. Zhang, W. Yu, and C. Zhou, Preparation of polysiloxane/perfluorosulfonic acid nanocomposite membranes in supercritical carbon dioxide

system for direct methanol fuel cell, International Journal of Hydrogen Energy 34 (2009) 6892-6901.

34. D. Chen, J. Nie, S. Yi, W. Wu, Y. Zhong, J. Liao, and C. Huang, Thermal behavior and mechanical properties of novel RTV silicon rubbers using divinyl-hexa(trimethoxysily)ethyl]-POSS as cross-linker, Polymer Degradation and Stability 95 (2010) 618-626.

35. S. Radi, S. Tighadouini, Y. Toubi, and M. Bacquet, Polysiloxane surface modified with bipyrazolic tripodal receptor for quantitative lead adsorption, Journal of Hazardous Materials 185 (2011) 494-501.

36. A. Durdureanu-Angheluta, M. E. Ignat, S.S. Maier, L. Pricop, A. Coroaba, A. Fifere, M. Pinteala, and A. Chiriac, Lipolytic biocatalyst based on recyclable magnetite-polysiloxane nanoparticles, Applied Surface Science 292 (2014) 898-905.

37. B. Pilch-Pitera, Polyurethane powder coatings containing polysiloxane, Progress in Organic Coatings 77 (2014) 1653-1662.

38. A. Ghanbari-Siahkali, S. Mitra, P. Kingshott, K. Almdal, C. Bloch, and H.K. Rehmeier, Investigation of the hydrothermal stability of cross-linked liquid silicone rubber (LSR), Polymer Degradation and Stability 90 (2005) 471-480.

39. T. Cui, Y.J. Chal, X.M. Chen, and J.W. Van Zee, Effect of water on life prediction of liquid silicone rubber seals in polymer electrolyte membrane fuel cell, Journal of Power Sources 196 (2011) 9536-9543.

40. J. Feng, Q. Zhang, Z. Tu, W. Tu, Z. Wan, M. Pan, and H. Zhang, Degradation of silicone rubbers with different hardness in various aqueous solutions, Polymer Degradation and Stability 109 (2014) 122-128.